



**HAL**  
open science

## Hydrogen generation by hydrolysis reaction using magnesium alloys with long period stacking ordered structure

Manuel Legrée, Véronique Charbonnier, Serge Al Bacha, Kohta Asano, Kouji Sakaki, Isabelle Aubert, Fabrice Mauvy, Jean-Louis Bobet

### ► To cite this version:

Manuel Legrée, Véronique Charbonnier, Serge Al Bacha, Kohta Asano, Kouji Sakaki, et al.. Hydrogen generation by hydrolysis reaction using magnesium alloys with long period stacking ordered structure. *International Journal of Hydrogen Energy*, 2021, 46 (71), pp.35161-35171. 10.1016/j.ijhydene.2021.08.087 . hal-03368335

**HAL Id: hal-03368335**

**<https://hal.science/hal-03368335>**

Submitted on 6 Oct 2021

**HAL** is a multi-disciplinary open access archive for the deposit and dissemination of scientific research documents, whether they are published or not. The documents may come from teaching and research institutions in France or abroad, or from public or private research centers.

L'archive ouverte pluridisciplinaire **HAL**, est destinée au dépôt et à la diffusion de documents scientifiques de niveau recherche, publiés ou non, émanant des établissements d'enseignement et de recherche français ou étrangers, des laboratoires publics ou privés.

# Hydrogen generation by hydrolysis reaction using Magnesium alloys with Long Period Stacking Ordered structure

M. Legrée<sup>a</sup>, V. Charbonnier<sup>b</sup>, S. Al Bacha<sup>c,d</sup>, K. Asano<sup>b</sup>, K. Sakaki<sup>b</sup>, I. Aubert<sup>e</sup>, F. Mauvy<sup>a</sup>, J.-L. Bobet<sup>a\*</sup>.

<sup>a</sup> CNRS, Univ. Bordeaux, Bordeaux INP, ICMCB, UMR 5026, F-33600 Pessac, France.

<sup>b</sup> National Institute of Advanced Industrial Science and Technology, 16-1 Onogawa, Tsukuba, Ibaraki 305-8569, Japan.

<sup>c</sup> Equipe de Recherche et d'Innovation en Electrochimie pour l'énergie (ERIEE), Institut de Chimie Moléculaire et des Matériaux d'Orsay (ICMMO), UMR CNRS 8182, Université Paris-Saclay, 91405 Orsay, France.

<sup>d</sup> Université Paris-Saclay, UMR CNRS 8180, Université de Versailles Saint-Quentin en Yvelines, Institut Lavoisier de Versailles, 45 Avenue des Etats-Unis, 78000 Versailles, France.

<sup>e</sup> University of Bordeaux, CNRS, Arts et Métiers Institute of technology, Bordeaux INP, INRAE, I2M Bordeaux, F-33400 Talence, France.

## Abstract

In the present work are reported the hydrogen generation performances of Long Period Stacking Ordered (LPSO) compounds with 18R, 14H and 10H-type structures by hydrolysis reaction in simulated seawater solution (35g/L NaCl). LPSO compounds and LPSO + Mg alloys synthesized by induction melting are described in the light of their microstructural and electrochemical properties. Except for 10H type, all LPSO present improved H<sub>2</sub> generation features compared to pure Mg. Indeed, 80% of the reaction is achieved in less than 40 minutes. The highest generation yield of 90% is obtained for single phase LPSO Mg<sub>87.6</sub>Ni<sub>5.5</sub>Y<sub>6.9</sub>. Alloys containing both Mg and LPSO beneficiate from galvanic coupling between the two phases leading to higher reactivity. The activation energies of 27.3 and 85.4 kJ/mol determined for Mg<sub>91</sub>Ni<sub>4</sub>Y<sub>5</sub> (14H+Mg) and Mg<sub>83.3</sub>Cu<sub>7.2</sub>Y<sub>9.5</sub> (18R) respectively clearly highlight this benefit from galvanic coupling.

**Keywords:** Magnesium, LPSO, Hydrogen generation, Hydrolysis, Corrosion

\* corresponding author: [jean-louis.bobet@u-bordeaux.fr](mailto:jean-louis.bobet@u-bordeaux.fr) (J.-L. Bobet).

## 1. Introduction

Long Period Stacking Ordered (LPSO) phases in magnesium based alloys have been reported for the first time by Inoue *et al.* in 2001 for the Mg-Zn-Y system [1]. Even though the crystallographic structure was not accurately described at the time, their study highlighted the interest of this new phase, conferring a high mechanical strength to the alloy. The improvement of magnesium alloys mechanical properties has thus been a motivation for extensive research on LPSO over the past two decades [2–4]. Along this period, common LPSO structures have been determined to be of the 10H, 18R, 14H or 24R type and were reported in various Mg – TM – RE (TM: Transition Metal, *e.g.* Cu, Ni, Zn, Al, Co) ; RE (Rare Earth, *e.g.* Y, Gd, Er, Sm) systems [5–7]. When it comes to alloy design, corrosion is a major challenge in terms of understanding the mechanisms and optimizing the performances. From this perspective, corrosion resistance behavior have been reported for alloys containing LPSO phases [8,9]. It has been shown that such phases can act both as (i) micro-cathodes that accelerate the corrosion of the less noble  $\alpha$ -Mg matrix through galvanic coupling and (ii) an anodic barrier hindering the propagation of the corrosion throughout the material [3,9–11]. Thus, the role of LPSO phase regarding magnesium alloys corrosion deserves deeper explorations.

In studies motivated by corrosion resistance enhancement, hydrogen evolution measurement is one way to determine the corrosion rate [12–15]. On the other hand, hydrogen generation studies (which are fundamentally similar to the former) focus more on an unusual perspective of corrosion efficiency and on the use of Mg based alloys as a mean for producing hydrogen [16–23]. The interest of this approach lays in economic reasons. Indeed, only high-grade magnesium scrap is recycled, which let most of the lower grade scraps with no valorization [24]. In this perspective, producing hydrogen by water hydrolysis with Mg alloys wastes (corresponding to their corrosion reaction at their equilibrium potential) has been proposed many times [25–30]. Up to now, studies mostly focused on optimizing reaction's yield and kinetics through alloy design or ball milling with various additives such as noble metals or salts [17,22,31,32].

To our knowledge, hydrogen production from LPSO phases and LPSO containing alloys have not been investigated yet. However, their features seem promising for producing hydrogen efficiently because LPSO compounds present high magnesium content and the presence of noble  $\text{TM}_6\text{RE}_8$  clusters in the structure may accelerate the hydrolysis reaction. Indeed, above-mentioned alloy design strategies (*Cf ref* [16,17]) consist in creating a maximized contact between Mg phase and a more noble phase in order to promote galvanic coupling. In such case, galvanic coupling occurs at the microstructural scale between two phases with different potentials and accelerates the alloy overall corrosion. In LPSO phases, the noble  $\text{TM}_6\text{RE}_8$  clusters (with nanometer dimension) are regularly

distributed in the magnesium structure itself: LPSO are made of alternated layers of Mg and layers of Mg +  $\text{TM}_6\text{RE}_8$  clusters. A potential nano-galvanic coupling occurring between these layers seems very interesting for enhanced  $\text{H}_2$  generation behavior. Thus, this work aims at exploring the hydrogen generation by hydrolysis with various LPSO compounds. Yttrium was chosen as the RE for its ability to form easily LPSO when melted with magnesium and TM. The nature of the TM may play an important role in hydrolysis reaction rate, for that reason two noble metals (*e.g.* nickel and copper) were compared. Finally, it appeared interesting to investigate the role of the structure by comparing different LPSO types: 10H, 18R and 14H. A series of alloys with high fraction of LPSO phase (namely, the [LPSO] alloys) are compared with a series of alloys containing LPSO phase and Mg as secondary phase (namely, [LPSO + Mg] alloys). The properties of these  $\text{H}_2$  production materials are compared and discussed in terms of composition, microstructure (SEM/EDXS) and electrochemical behavior.

## 2. Materials and methods

The compounds involved in the present study were synthesized using chunks of magnesium (99.9%) from Kojundo Chemical Laboratory Co., Ltd., copper (99.99%) and nickel (99.9%) from Furuuchi Chemical Co., and yttrium (99.9%) from Nippon Yttrium Co., Ltd. The elements were melted together in an induction furnace under a helium atmosphere. Due to its high vapor pressure, an excess of 7 wt.% of Mg was added. The obtained ingots were subsequently annealed under argon atmosphere at 400°C in an aluminum foil or at 500°C in a tantalum foil. The detailed annealing conditions are given in Table 1.

Pristine samples and hydrolysis reaction products were systematically characterized by X-ray diffraction (XRD) using a Philips PANalyticalX'Pert (PW1820) diffractometer with Cu  $\text{K}\alpha_1$  radiation ( $\lambda=1.5405 \text{ \AA}$ ). Scanning Electron Microscopy (SEM) observations were made using a TESCAN VEGA3 SB and SERON TECHNOLOGY microscopes equipped with secondary electron and back scattered electron detectors (hereafter referred to as SE and BSE modes respectively). Furthermore, the elemental composition of the surface was analyzed using an energy dispersive X-ray (EDXS) detector.

Hydrolysis reactions were carried out in a closed 100 mL three-neck round bottom flask connected to a burette that dips in a beaker of water. The experimental setup was previously described in ref [33]. Water from the beaker is initially sucked up into the burette. Then, the hydrogen produced during the experiment causes water displacement back to the beaker and a balance connected to a computer records the mass variation; allowing to follow in real time the hydrogen generation. Bulk samples were filed and about 30 mg of material were taken to react with 20 mL of simulated seawater solution (*i.e.*

35 g/L NaCl). The solution was rapidly stirred with a magnetic bar and during the whole experiment the temperature was kept at a constant temperature of 25°C. After measurement, 10 mL of 0.5 M HCl were added to complete the hydrolysis process and thereby generate the maximum H<sub>2</sub> amount the sample could release. The yield of reaction was obtained from this amount of H<sub>2</sub>.

Open circuit potential (OCP) and potentiodynamic polarization measurements were led in the same simulated seawater solution at room temperature with a three electrodes set-up (Working electrode: studied sample, Counter electrode: Titanium net; Reference electrode: Saturated Calomel Electrode (SCE) - Hg/Hg<sub>2</sub>Cl<sub>2</sub>). These electrodes were linked to a VersaSTAT 4 potentiostat and controlled via VersaStudio software. The bulk samples were abraded up to 4000 grit SiC with ethanol as lubricant prior to each electrochemical test. Polarization curves were obtained after 40 min open circuit potential stabilization solution (*i.e.* until a constant OCP is reached). Anodic and cathodic polarization curves were recorded separately with a scan rate of 0.5 mV/s as follows: (i) a first sweep from +50 mV to -250 mV vs OCP for the cathodic curve and (ii) from -50 mV to +250 mV vs OCP for the anodic polarization measurement.

### 3. Results and discussion

#### 3.1. Materials characterization

LPSO compounds based on Mg-TM-Y (TM= Ni, Cu) with different Mg contents were synthesized. In this work, XRD analysis was used for LPSO structure type determination and secondary phases identification. It can be consulted in supplementary materials section (figures S1 & S2). In each section, the results for [LPSO] alloys are discussed firstly and the [LPSO + Mg] alloys (*i.e.* Mg<sub>91</sub>Ni<sub>4</sub>Y<sub>5</sub>) are presented after.

Figure 1a displays the SEM micrographs of Mg<sub>80.6</sub>Ni<sub>8.3</sub>Y<sub>11.1</sub> alloy annealed at 400°C for 50 hours (hereafter referred to as 10H-Ni). XRD analysis shows that it forms 10H LPSO (Figure S1). Both Mg<sub>83.3</sub>Cu<sub>7.2</sub>Y<sub>9.5</sub> (figure 1b) and Mg<sub>87.6</sub>Ni<sub>5.5</sub>Y<sub>6.9</sub> (figure 1c) formed 18R LPSO after annealing 400°C for 50 hours and at 500°C for 10 days, respectively (identified by XRD as shown in figure S1 and named respectively 18R-Cu and 18R-Ni). White spots can be seen on BSE-SEM of figure 1 and are identified as yttrium oxide in the case of 10H-Ni (*i.e.* Mg<sub>80.6</sub>Ni<sub>8.3</sub>Y<sub>11.1</sub>). For the two other compounds some spots have shown a high yttrium content based on EDXS quantifications while some others correspond to Mg<sub>2</sub>Ni and Mg<sub>2</sub>Cu phases (in respective alloys), which was confirmed by XRD. The light grey phase in 18R-Cu (Mg<sub>83.3</sub>Cu<sub>7.2</sub>Y<sub>9.5</sub>) was identified as Mg<sub>4</sub>YCu based on EDXS measurements (figure 1b).

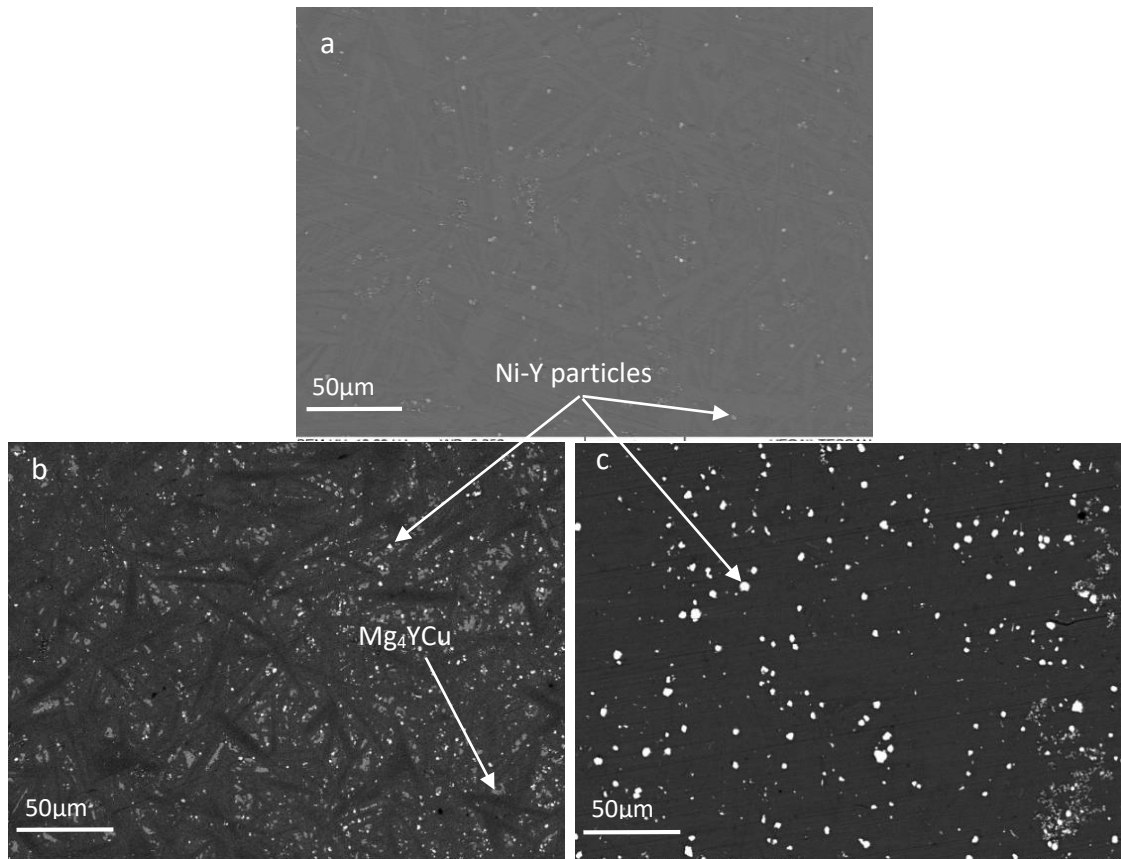


Figure 1 Backscattered Electrons (BSE) - SEM micrographs of LPSO compounds: (a) 10H-Ni ( $Mg_{80.6}Ni_{8.3}Y_{11.1}$ ), (b) 18R-Cu ( $Mg_{83.3}Cu_{7.2}Y_{9.5}$ ) and (c) 18R-Ni ( $Mg_{87.6}Ni_{5.5}Y_{6.9}$ ).

A stripe-like microstructure is observable with a very low contrast on figures 1a & 1c which is characteristic of alloys with high LPSO phase content [34,35] and goes with slight EDXS compositions variations. In the 18R-Cu ( $Mg_{83.3}Cu_{7.2}Y_{9.5}$ ) compound, the dark areas present an average composition of  $Mg_{87}Cu_6Y_7$ , while the bright ones have an average close to  $Mg_{83.6}Cu_{7.4}Y_9$ . This observation has already been discussed elsewhere [36,37]. Explanations involved Mg insertion or substitution in  $TM_6RE_8$  clusters and full  $TM_6RE_8$  substitution by Mg. LPSO inhomogeneity is however not systematic since 18R-Ni ( $Mg_{87.6}Ni_{5.5}Y_{6.9}$ ) does not exhibit such feature (figure 1c): the higher annealing temperature for this sample may have play a key role.

$Mg_{91}Ni_4Y_5$  alloys formed a mixture of  $\alpha$ -Mg and LPSO phases (figure 2). For this reason, this series of three samples will be referred as [LPSO + Mg] alloys. In these series, the LPSO phases were found to be of 14H- and 18R-type when annealed at 500°C and 400°C respectively (identified from XRD, Cf figure S2). As expected, better homogeneity is obtained when the material was annealed at 500°C. At 400°C, extend annealing time from 50h (figure 2b) to 10 days (figure 2c) tends to homogenize the LPSO phase (with EDXS estimation shots varying from 91 at.% to 93 at.% of Mg for 10 days, against 89 at.% to 93 at.% of Mg for 50h). However, the overall microstructure remained divided into  $\alpha$ -Mg and LPSO phases. By comparing figures 1 and 2, one can notice that less white spots (identified as

Mg<sub>2</sub>Ni from XRD and EDXS) are observed for these compounds with higher Mg content (*i.e.* for the [LPSO + Mg] alloys).

Mg surface proportions have been estimated with ImageJ software to be 15, 12 and 18% for 500°C 10d (figure 2a), 400°C 50h (figure 2b) and 400°C 10d (figure 2c) respectively with accuracy of about 1%. Imaging technique was used for phase proportions estimation since exploiting XRD data with preferred orientation would lead to less accurate results. In addition, composition analysis showing a LPSO stoichiometry varying locally from the theoretical one, a Rietveld refinement would not give meaningful phase fractions. To have an idea of this stoichiometry variation, the LPSO composition range given in table 1 has to be compared to the theoretical values of 10H, 14H and 18R, which are Mg<sub>76.7</sub>TM<sub>10</sub>RE<sub>13.3</sub>, Mg<sub>83.3</sub>TM<sub>7.2</sub>RE<sub>9.5</sub> and Mg<sub>80.6</sub>TM<sub>8.3</sub>RE<sub>11.1</sub> respectively [36,37]. From this comparison, it is clear that the LPSO phases of the herein studied samples are all Mg over-stoichiometric.

Series	Name	Nominal composition	Annealing conditions	Phase identification (Both XRD &EDXS)	Extra phases (SEM)	LPSO composition range (EDXS)	Mg surface proportion (ImageJ)	LPSO theoretical composition
[LPSO] alloys	10H-Ni	Mg <sub>80.6</sub> Ni <sub>8.3</sub> Y <sub>11.1</sub>	400°C 50h	10H	Y <sub>2</sub> O <sub>3</sub>	Mg <sub>85</sub> Ni <sub>5</sub> Y <sub>10</sub> - Mg <sub>83</sub> Ni <sub>6</sub> Y <sub>11</sub>	0%	10H : Mg <sub>76.7</sub> TM <sub>10</sub> RE <sub>13.3</sub>
	18R-Cu	Mg <sub>83.3</sub> Cu <sub>7.2</sub> Y <sub>9.5</sub>	400°C 50h	18R ; Mg <sub>2</sub> Cu	Y <sub>2</sub> O <sub>3</sub> ; Y ; Mg <sub>4</sub> YCu	Mg <sub>87</sub> Cu <sub>6</sub> Y <sub>7</sub> - Mg <sub>83.6</sub> Cu <sub>7.4</sub> Y <sub>9</sub>	0%	18R : Mg <sub>80.6</sub> TM <sub>8.3</sub> RE <sub>11.1</sub>
	18R-Ni	Mg <sub>87.6</sub> Ni <sub>5.5</sub> Y <sub>6.9</sub>	500°C 10d	18R ; Mg <sub>2</sub> Ni	Y <sub>2</sub> O <sub>3</sub> ; Y	Mg <sub>90</sub> Ni <sub>4</sub> Y <sub>6</sub>	0%	
[LPSO +Mg] alloys	14H+Mg (500 °C 10d)	Mg <sub>91</sub> Ni <sub>4</sub> Y <sub>5</sub>	500°C 10d	Mg ; 14H ; Mg <sub>2</sub> Ni	-	Mg <sub>92</sub> Ni <sub>3</sub> Y <sub>5</sub>	15%	14H : Mg <sub>83.3</sub> TM <sub>7.2</sub> RE <sub>9.5</sub>
	18R+Mg (400 °C 10d)		400°C 50h	Mg ; 18R ; Mg <sub>2</sub> Ni	-	Mg <sub>93</sub> Ni <sub>3</sub> Y <sub>4</sub> - Mg <sub>91</sub> Ni <sub>3.6</sub> Y <sub>5.4</sub>	12%	18R : Mg <sub>80.6</sub> TM <sub>8.3</sub> RE <sub>11.1</sub>
	18R+Mg (400 °C 50h)		400°C 10d	Mg ; 18R ; Mg <sub>2</sub> Ni	-	Mg <sub>91</sub> Ni <sub>3.5</sub> Y <sub>5.5</sub> - Mg <sub>90</sub> Ni <sub>4</sub> Y <sub>6</sub>	18%	

Table 1 Different investigated compounds and their corresponding heat treatments and physico-chemical analysis.

The information obtained from the characterization techniques is summarized in table 1. It has to be noted that the presence of phases other than LPSO or Mg may give different hydrolysis performances and electrochemical results than if pure LPSO compounds were tested. These samples are the result of optimized synthesis conditions and synthesis of 100% pure LPSO phase is very difficult to achieve without precipitation of small amounts of these extra phases. Indeed, Mg, Y, Mg<sub>2</sub>Ni or Mg<sub>24</sub>Y<sub>5</sub> are stable phases which can be easily formed during the synthesis.

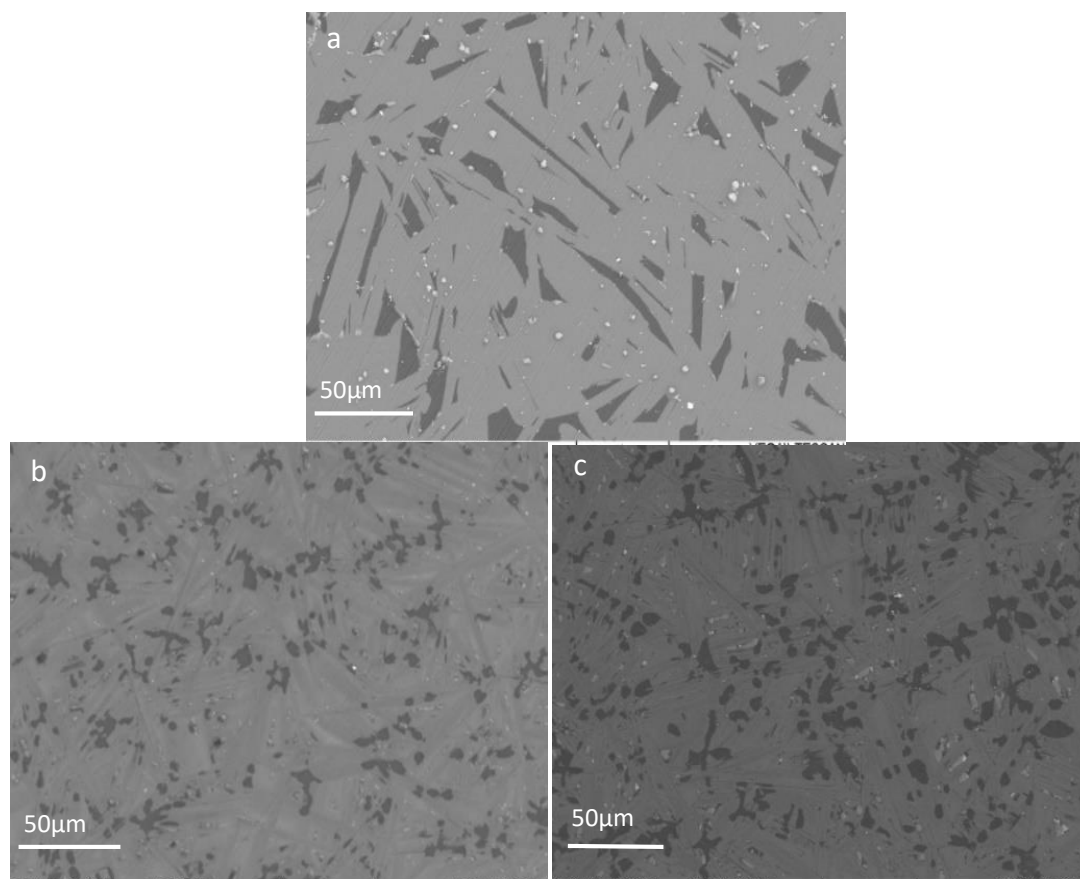


Figure 2 BSE-SEM micrographs of [LPSO + Mg] compounds Mg<sub>91</sub>Ni<sub>4</sub>Y<sub>5</sub>: (a) 14H+Mg (500°C 10d), (b) 18R+Mg (400°C 50h) and (c) 18R+Mg (400°C 10d).

### 3.2. Hydrolysis reaction

The studied ingots were filed to make small pieces for hydrolysis reactions. In the literature, most studies use whether (i) bulk material to characterize an alloy corrosion properties or (ii) powders in order to get optimized reactivity for hydrogen generation [38–42]. Measuring hydrogen generation from shavings (which have relatively large size) may not show the best performances compared to powders because of less important specific surface areas. On the other hand, it takes into account the economic constraints: coarse particles are easier to produce than powders and more relevant for

producing hydrogen at a reasonable price. In addition, since Mg powder is flammable, coarse particles are easier to handle in practical applications. Based on these reasons, the filed particles were used to evaluate hydrolysis performance of LPSO based compounds.

All samples presented a similar particle size and morphology after being filed for hydrolysis experiment. Typical example is given in figure 3 with the alloy 18R+Mg ( $Mg_{91}Ni_4Y_5$  400°C 50h). The secondary electron micrographs show flat particles with a smooth surface and a ribbed one. The filed particles have relatively large dimensions ranging from tens to some hundreds of micrometers. The evaluation of material density showed no significant difference between measured values and theoretical ones, indicating that no closed porosity was present in the filed samples. This is important to know since a particle with pores would present faster kinetics due to a greater contact surface with water during the reaction.

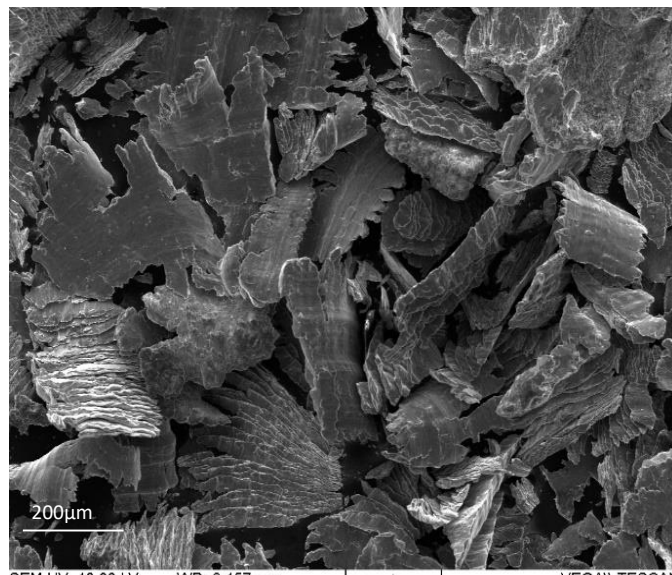


Figure 3 Secondary Electrons (SE)-SEM micrograph of filed 18R+Mg ( $Mg_{91}Ni_4Y_5$  400°C 50h).

The reaction progress plotted in figures 4 and 5 is calculated from the hydrogen yield obtained from the total volume generated after addition of 10 mL of 0.5M HCl to the reaction medium. In figure 4, an important kinetic difference can be seen between 10H and 18R compounds. The cluster chemical composition could be the reason for different coupling efficiency with the Mg-rich parts. Indeed, the highest the TM content, the highest the apparent potential of the cluster and the more efficient the coupling (observation discussed and proven at the macroscopic scale in section 3.3). The TM/RE ratio obtained from EDXS measurements are 0.5 to 0.55 and 0.67 for 10H-Ni ( $Mg_{80.6}Ni_{8.3}Y_{11.1}$ ) and 18R-Ni ( $Mg_{87.6}Ni_{5.5}Y_{6.9}$ ) respectively. The hydrolysis results follow this trend of a higher TM/RE ratio implying a faster reaction. Another possible explanation is the average distance between Mg—TM—RE layers (*i.e.* containing the  $TM_6RE_8$  clusters). This factor would impact the local nano-galvanic coupling that is

supposed to occur between layers of HCP-Mg and Mg—TM—RE layers. Charbonnier *et al.* have calculated interplanar distance ( $d_{002}$ ) of 1.3 and 1.56 nm [36] for 10H (calculated from structure proposed in [43]) and 18R [37] respectively. From our results, it would mean that the higher the distance between Mg—TM—RE layers, the more efficient the corrosion (or at least that an optimum distance exists). One last reason for this observation can be proposed at the microstructural scale as 10H-Ni ( $\text{Mg}_{80.6}\text{Ni}_{8.3}\text{Y}_{11.1}$ ) alloy contains less Ni-Y particles than 18R-Cu ( $\text{Mg}_{83.3}\text{Cu}_{7.2}\text{Y}_{9.5}$ ) and 18R-Ni ( $\text{Mg}_{87.6}\text{Ni}_{5.5}\text{Y}_{6.9}$ ), again leading to less galvanic coupling. The difference in kinetics between 18R-Cu ( $\text{Mg}_{83.3}\text{Cu}_{7.2}\text{Y}_{9.5}$ ) and 18R-Ni ( $\text{Mg}_{87.6}\text{Ni}_{5.5}\text{Y}_{6.9}$ ), can be understood by the different TM used, Mg-TM galvanic cells being more efficient with Ni ( $\Delta E = 1.52\text{V}$ ) than with Cu ( $\Delta E = 1.38\text{V}$ ).

After 40 minutes, the reaction yields (before acid addition) for [LPSO] alloys were 87.5 %, 74.3% and 33.1% for 18R-Ni ( $\text{Mg}_{87.6}\text{Ni}_{5.5}\text{Y}_{6.9}$ ), 18R-Cu ( $\text{Mg}_{83.3}\text{Cu}_{7.2}\text{Y}_{9.5}$ ) and 10H-Ni ( $\text{Mg}_{80.6}\text{Ni}_{8.3}\text{Y}_{11.1}$ ) respectively. These values are to be compared with that of pure Mg, whose yield equals 30 % after 40 minutes of hydrolysis. In addition, it has to be noted that yttrium can significantly contribute to hydrogen production since pure yttrium has been tested separately and showed a yield of 300 mL of  $\text{H}_2/\text{g}$  after 10 minutes of reaction in the same conditions (*e.g.* 3 times lower than the one of Mg or LPSO). In terms of reaction yield, LPSO compounds have an enhanced  $\text{H}_2$  production compared to pure Mg on the long run (figure 4), this can be assigned to the presence of electrochemically noble clusters (cathodic behavior) that enhances the corrosion through galvanic coupling with less noble Mg (behaving as an anode).

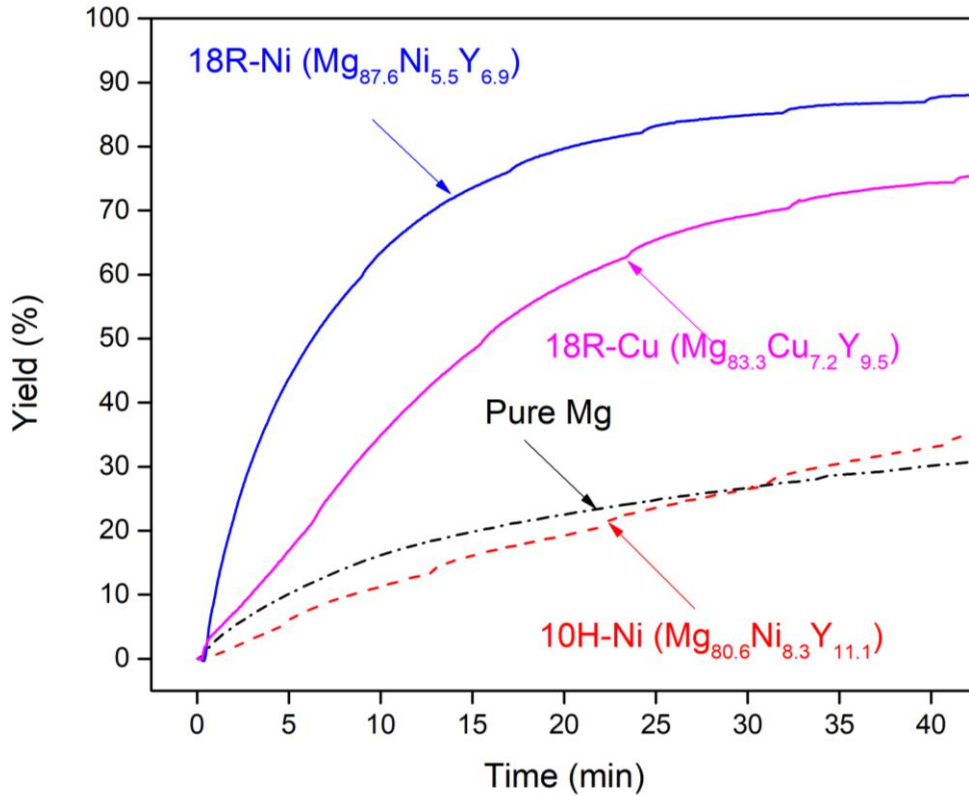


Figure 4 Hydrogen generation by hydrolysis reaction at 25°C for LPSO compounds compared with pure Mg.

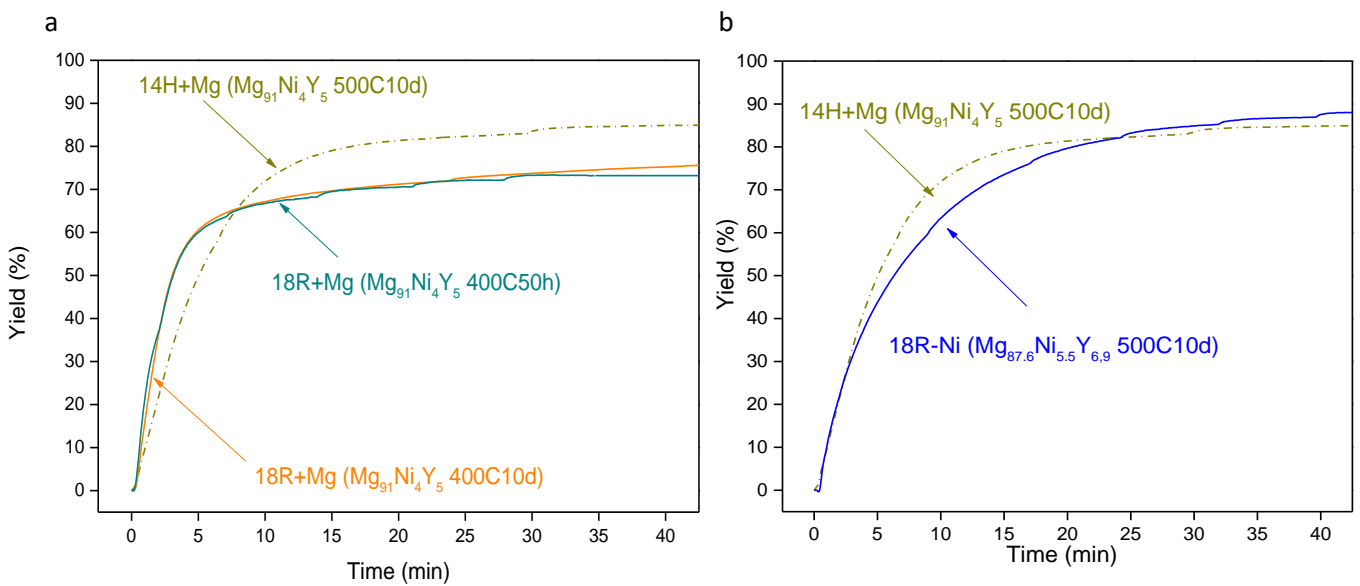


Figure 5 Hydrogen generation by hydrolysis reaction at 25°C for (a) Mg + LPSO alloys ( $Mg_{91}Ni_4Y_5$ ) with different annealing conditions and (b) comparison with 18R-Ni ( $Mg_{87.6}Ni_{5.5}Y_{6.9}$ ).

Figure 5a shows that [LPSO + Mg] samples ( $Mg_{91}Ni_4Y_5$ ) annealed at 400°C have a higher kinetic than the one annealed at 500°C. Two possible reasons for the higher reactivity (kinetic) of 400°C (18R) compounds compared to the 500°C (14H) may be:

- the overall inhomogeneity in the chemical composition of the 18R-type LPSO phase that leads to more possible galvanic cells (Cf Table 1 and figure 2)
- the Mg phase is more spread in the 400°C annealed samples (Cf figure 2) offering a larger LPSO-Mg contact (thus increasing interphase interactions).

The interplanar explanation proposed above for compounds containing LPSO only, does not follow the same logic here between 18R and 14H ( $d_{002}$  of 1.56 and 1.8 nm respectively [36]). However, in this case, the presence of the two phases may be more determining for the corrosion rate compared to the structural features. Indeed, better kinetics are observed for the [LPSO + Mg] alloys than for [LPSO] alloys (figure 5b compares fastest [LPSO] and slowest [LPSO + Mg]). This is due to galvanic coupling between LPSO and Mg phase. For the 400°C-annealed compounds, the LPSO homogenization obtained from increasing the annealing time from 50h (figure 2b) to 10 days (figure 2c) did not result in any difference in the hydrolysis behavior (figure 5a).

$Mg_{91}Ni_4Y_5$  annealed at 500°C shows a better yield than the samples annealed at 400°C (figure 5a). The Mg phase proportion is different for 18R + Mg (400°C 10d) (18% surface estimation) and for 18R + Mg (400°C 50h) (12%), but their total  $H_2$  production is identical. In addition, Mg phase fraction equals 15% for 18R + Mg (500°C 10d), which is in between the two samples annealed at 400°C. This indicates that this parameter cannot explain the final yield difference with the 14H + Mg (500°C 10d) seen in figure 5a. Additionally, it is very likely that all the Mg phase is consumed during the reaction because of its higher ability to corrode compared to more noble LPSO phase. The nature of the LPSO structure neither seems to explain the difference in yield between  $Mg_{91}Ni_4Y_5$  annealed at 400°C and 500°C since figure 5b shows that both 14H and 18R compounds can deliver high yield.

As previously mentioned, the cluster composition could be the determining parameter for the final yield. In fact, different cluster compositions are susceptible to be obtained by insertion and/or substitution. Thus, the final reaction yield may be determined by the ability of the Mg involved in the cluster to react with water (*i.e.* corrosion of these different possible clusters types).

In figure 6, X-ray diffraction patterns of 18R+Mg ( $Mg_{91}Ni_4Y_5$  400°C 50h) after 5 minutes and 1 hour hydrolysis show the formation of  $Mg(OH)_2$  with broad peaks, indicating the low crystallinity of this reaction product. It is clearly seen that most of the reaction has been completed in the first five minutes, where most of the  $Mg(OH)_2$  was formed and LPSO peaks strongly diminished. A slight intensity decrease is observed for the LPSO peaks between 5 minutes and 1 hour of hydrolysis but two peaks still remain after 1 hour, attesting for the non-completion of the reaction. These observations are in good agreement with the hydrogen generation curve (figure 5a) where a rapid  $H_2$  generation is seen in the first 5 minutes followed by a slow stabilization and a limited total production. The intensity

of LPSO peaks after one hour may appear relatively low knowing the final yield of 75% for this compound (figure 5a). Reasons for this are the low crystallinity of the remaining powder and the presence of  $Mg(OH)_2$  covering the surface of unreacted LPSO. Mg phase related peaks disappeared right after the 5 first minutes of reaction while the LPSO phase peaks still remain after 1 hour. This observation reinforces the idea that Mg reacts completely and that the final generation yield depends on the composition and the microstructure of the LPSO phase. With the low crystallinity of the powder after hydrolysis reaction it is difficult to say if the  $Mg_2Ni$  initially present has reacted or not. Peak at  $2\theta = 20^\circ$  can indeed be hidden by broad  $Mg(OH)_2$  peak at  $2\theta = 18^\circ$ .

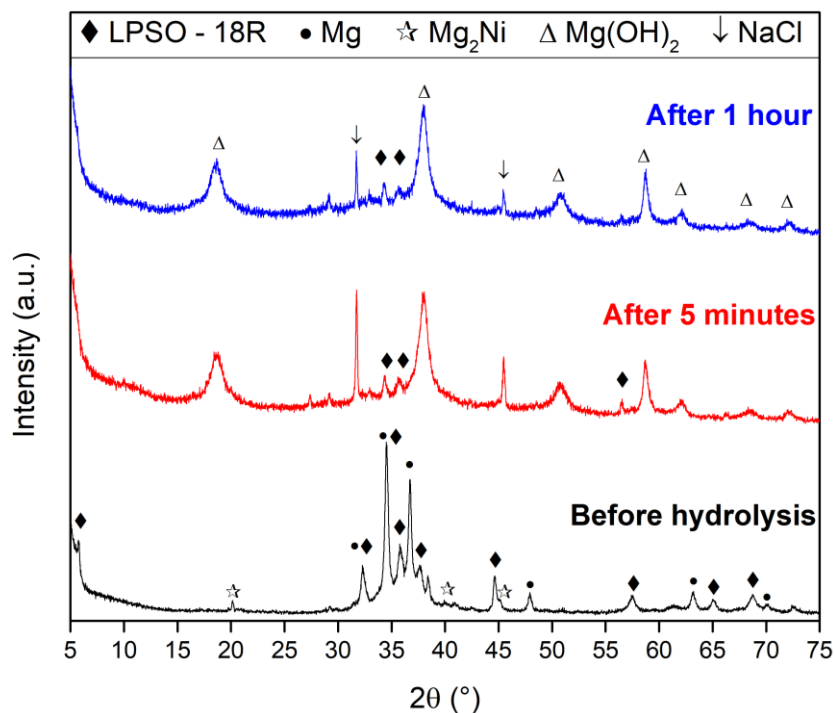


Figure 6 X-Ray diffraction pattern of 18R + Mg ( $Mg_{91}Ni_4Y_5$  400°C 50h) before (bottom, black), after 5 min (middle, red) and 1 hour (top, blue) hydrolysis.

Figure 7 shows the surface of 14H + Mg ( $Mg_{91}Ni_4Y_5$  500°C 10d) compound after 30 seconds immersion in simulated seawater solution. It presents corrosion points located on the Mg phase only. Galvanic coupling is thus occurring between Mg and 14H phases, favoring corrosion of Mg (anode) at first and of the overall material after propagation from these corrosion initiation sites.

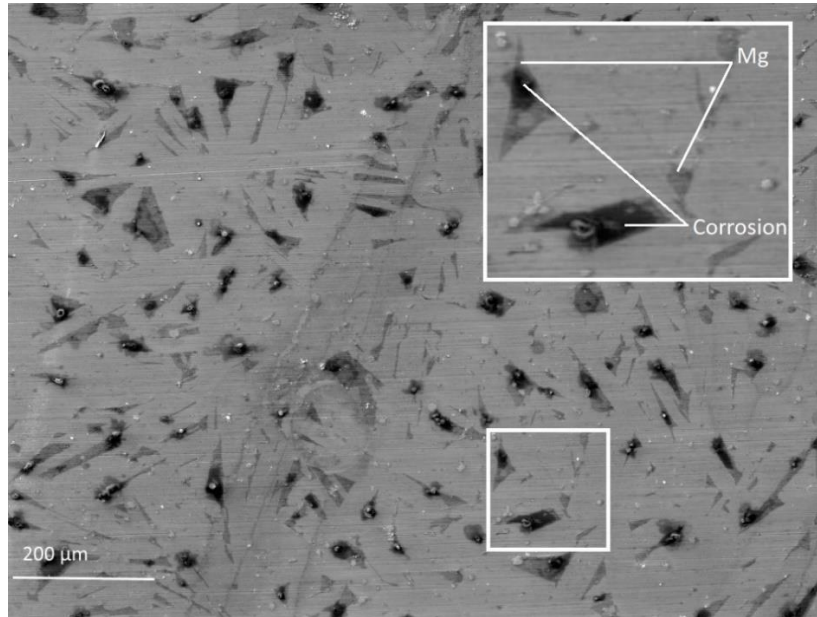


Figure 7 BSE-SEM micrograph of bulk 14H+Mg ( $Mg_{91}Ni_4Y_5$  500°C 10d) surface after 30 seconds of immersion in 35g/L NaCl solution.

Avrami-Erofeev equation has been widely used to fit hydrogen generation curves versus time and obtain reaction rate constants [38,40,41]. When this latter is obtained at different temperatures, it allows activation energy determination using Arrhenius law. Considering the shape of the hydrogen generation curves obtained here with LPSO compounds (figures 4 & 5), this model appears to be relevant except for 10H ( $Mg_{80.6}Ni_{8.3}Y_{11.1}$ ) that has a quasi-linear evolution. Hydrolysis experiments were conducted at 0, 17, 25, 40 and 60°C and equation (1) was fitted to get n and k constants:

$$\ln[-\ln(1-F)] = \ln k + n \times \ln t \quad (1)$$

with F the generated hydrogen volume fraction, t the reaction time (s), n the constant relative to the reaction mechanism and k the reaction rate constant.

For 18R+Mg ( $Mg_{91}Ni_4Y_5$  400°C 50h) and 18R-Ni ( $Mg_{87.6}Ni_{5.5}Y_{6.9}$ ) the rate constants obtained at the different mentioned temperatures did not allow determining a meaningful activation energy value. However, rate constants obtained for 18R+Mg ( $Mg_{91}Ni_4Y_5$  400°C 50h) were very close at the different temperatures which indicates that it has a very low activation energy (*i.e.* small  $\ln(k)=f(1/T)$  slope). In fact, even at 0°C, rapid hydrolysis reaction was observed. On the other hand, values of 27.3 and 85.4 kJ/mol were obtained for 14H+Mg ( $Mg_{91}Ni_4Y_5$  500°C 10d) between 0°C and 60°C and 18R-Cu ( $Mg_{83.3}Cu_{7.2}Y_{9.5}$ ) between 17°C and 60°C respectively. Typical activation energy reported for hydrolysis of ball milled magnesium alloys ranges from 40 to about 10 kJ/mol for the lowest ones [31,38,40,42]. While the activation energy of 18R-Cu ( $Mg_{83.3}Cu_{7.2}Y_{9.5}$ ) is higher than these values (lower hydrolysis performances) the one of 14H+Mg ( $Mg_{91}Ni_4Y_5$  500°C 10d) is in the same range whereas in our study the compound did not benefit from important mechanical surface activation. Even without ball milling,

hydrolysis of [LPSO + Mg] alloys presents a very high rate. This is especially the case for 18R+Mg ( $\text{Mg}_{91}\text{Ni}_4\text{Y}_5$  400°C 50h) for which Arrhenius relation slope is so small that it could not be determined accurately. As for the hydrolysis kinetics, important difference is observed between [LPSO] and [LPSO + Mg] alloys. These differences in reactivity were further studied through electrochemical measurements to better reveal the correlation between the composition and the microstructure of Mg-based compound and their hydrolysis/corrosion reactivity.

### 3.3. Electrochemical measurements

Ingots were used for electrochemical measurements in order to characterize their chemical reactivity (reaction taking place on a known surface area). The Open Circuit Potentials (OCP) of the different compounds plotted in figure 8a stabilize after 5 to 10 minutes of immersion. In order to ensure being in steady state conditions, the polarization experiments exposed below are conducted after 40 minutes of immersion in simulated seawater solution. The electrochemical noise and the shape of recorded OCP curves versus time are specific to each alloy since they were the same for the five measurements done on each sample. If it shows that each compound undergoes different surface reaction mechanisms, it is difficult to deduce more information from this sole measure.

Figure 8a shows that even with a smaller Mg content, the 18R-Cu ( $\text{Mg}_{83.3}\text{Cu}_{7.2}\text{Y}_{9.5}$ ) shows a lower potential (-1.34V/SCE) than 18R-Ni ( $\text{Mg}_{87.6}\text{Ni}_{5.5}\text{Y}_{6.9}$ ) (-1.24V/SCE). This result can be understood knowing that Cu is less noble than Ni, this statement can also explain the difference in hydrolysis kinetic (figure 4) found between these two compounds (*i.e.* lesser galvanic coupling effect with smaller  $\Delta E$  between Mg and TM).

Figure 8b shows that a linear decrease of the potential is observed with increasing the magnesium content. This result was predictable since the potentials of Ni and Y are higher than that of Mg and already observed in previous study [16]. When OCP values of the Ni containing compounds are plotted versus Mg content and extrapolated to 100%wt. Mg, a value of -1.66V/SCE is obtained, which is in good agreement with the value of -1.65V/SCE reported in the literature in the same conditions [16]. Note that for the fitting curve of figure 8b only Ni containing alloys were considered and a supplementary alloy was measured to obtain the 90%wt. Mg point:  $\text{Mg}_{97}\text{NiY}_2$ . The black points are the points used for fitting and a star was added to show the OCP value for Mg found in the literature in the same conditions.

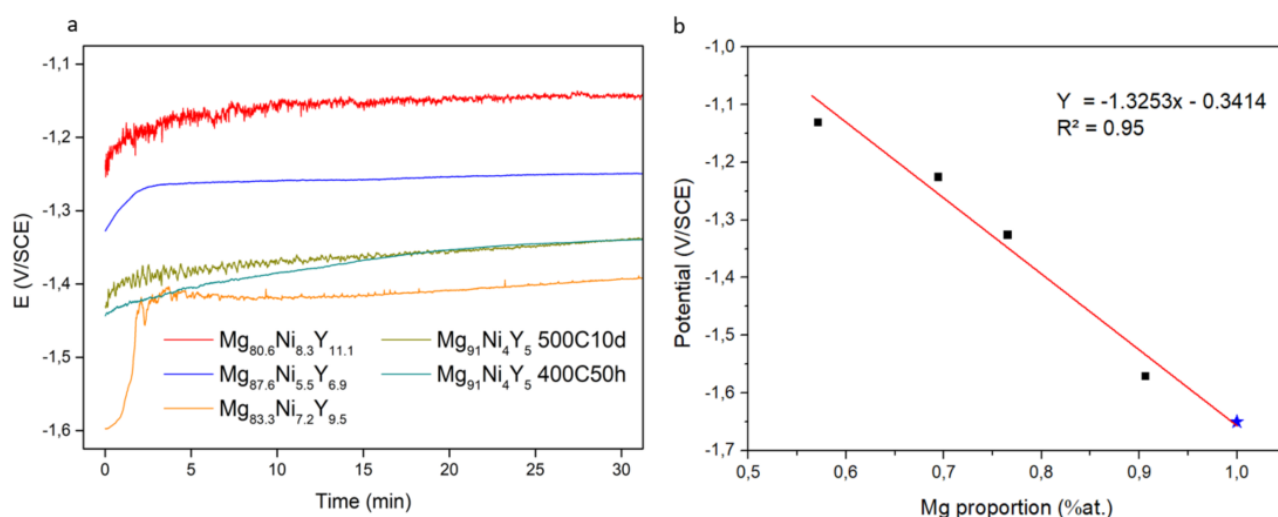


Figure 8 (a) Open Circuit Potentials (OCP) at 25°C in 35g/L NaCl solution and (b) linear fit of OCP variation with Mg content (black points : OCP after 40 minutes; blue point pure Mg from [16]).

The Tafel extrapolation method was used to determine the corrosion current density and consequently the surface electrochemical reactivity of the studied compounds. The method relies on a geometrical construction of Tafel linear branch on potentiodynamic polarization data (figure 9a) that allow the estimation of  $J_{corr}$  values. In order to limit the inherent uncertainty linked to the Tafel construction and normalize all the measurements, tangents were drawn to fit best in the range +/- 100mV vs OCP (See the vertical dashed lines on figure 3a , supplementary materials) to the end of the curve. Moreover at least four polarization curves were done on each sample. The anodic and cathodic branches were performed separately to avoid measuring the anodic part of the curve with surface and medium being previously modified during the cathodic polarization. An idea of the uncertainty in these measurement with the example of 14H+Mg (Mg<sub>91</sub>Ni<sub>4</sub>Y<sub>5</sub> 500°C 10d) is highlighted in figure 3b (Supplementary materials). In this case, anodic and cathodic  $E_{corr}$  are shifted by about 25mV which lead a minimum of 10% error on the  $J_{corr}$  value (Cf table 2). All the measurements were made by the same operator and most of the repeated tests shared the same incertitude interval, therefore, a reliable comparison between the compounds is possible.

The values reported in table 2 show that a higher corrosion rate is obtained for compounds with higher Mg content. This tendency is the same as the kinetics observed from the hydrolysis curves. Moreover, it confirms that 18R+Mg (Mg<sub>91</sub>Ni<sub>4</sub>Y<sub>5</sub> 400°C 50h) is more reactive than 14H+Mg (Mg<sub>91</sub>Ni<sub>4</sub>Y<sub>5</sub> 500°C 10d). This indicates that the surface corrosion rate is the determining factor in our hydrolysis experiment. Presence of two phases in Mg<sub>91</sub>Ni<sub>4</sub>Y<sub>5</sub> compounds is the reason for fastest reaction compared to the case where all Mg is involved in LPSO phase, offering opportunity of interphase corrosion and galvanic coupling between the two phases. This tendency of increasing corrosion rate with Mg content has already been reported in the same conditions by Alasmar *et al.* for Mg rich alloys

in the Nd-Ni-Mg system [16]. The investigated alloys consisted of NdNiMg<sub>15</sub> and Mg phase with different Mg phase fraction, a microstructural understanding of the results was proposed.  $J_{corr}$  values obtained were close to those presented in this present work. The comparison between pure NdNiMg<sub>15</sub> and pure 18R-Ni (Mg<sub>87.6</sub>Ni<sub>5.5</sub>Y<sub>6.9</sub>) compounds is especially interesting since both materials have the same Mg atomic proportions and very close OCP values (-1.23 V/SCE for NdNiMg<sub>15</sub> [16] and -1.25 V/SCE for Mg<sub>87.6</sub>Ni<sub>5.5</sub>Y<sub>6.9</sub> respectively). Dissimilarities are the nature of the rare earth (Nd or Y) and the crystallographic structure: TM-RE atoms are regularly distributed along tunnels in the structure of the first (Space group: P4/nmm) while in the LPSO phases they form clusters (Space group: P3<sub>2</sub>12) [37,44].  $J_{corr}$  value of 1.7 mA/cm<sup>2</sup> is given for NdNiMg<sub>15</sub>, against 1.3mA/cm<sup>2</sup> for 18R-Ni (Mg<sub>87.6</sub>Ni<sub>5.5</sub>Y<sub>6.9</sub>)[16]. Given the previous remarks on the method uncertainty, the corrosion rate of these Mg rich RE-TM-Mg compounds does not appear significantly different. Regarding the kinetics, the nature of the rare earth and the differences in crystallographic structure do not appear to be first-order parameters, unlike differences in OCP and Mg content.

Compound	$J_{corr}$ (mA/cm <sup>2</sup> )	Number of measurements
10H-Ni (Mg <sub>80.6</sub> Ni <sub>8.3</sub> Y <sub>11.1</sub> )	0.30 ± 0.05	5
18R-Cu (Mg <sub>83.3</sub> Cu <sub>7.2</sub> Y <sub>9.5</sub> )	1.0 ± 0.1	5
18R-Ni (Mg <sub>87.6</sub> Ni <sub>5.5</sub> Y <sub>6.9</sub> )	1.3 ± 0.2	8
14H+Mg (Mg <sub>91</sub> Ni <sub>4</sub> Y <sub>5</sub> 500°C 10d)	2.1 ± 0.2	4
18R+Mg (Mg <sub>91</sub> Ni <sub>4</sub> Y <sub>5</sub> 400°C 50h)	2.9 ± 0.6	4

Table 2 Corrosion current densities obtained from Tafel extrapolation method.

#### 4. Conclusion

Alloys containing LPSO phase were investigated in order to evaluate their potential for hydrogen production by hydrolysis. The LPSO phases are attractive for this application because they are Mg-rich, but also because they contain transition metal (TM) and rare earth (RE) that may accelerate the reaction. Here, Ni or Cu was chosen as TM and Y as the RE. Two series of samples were synthesized: the first series are samples with high content of LPSO phase, whereas the second series also contains a relatively large amount of Mg phase (12 to 18%). Their properties of hydrogen generation by hydrolysis were evaluated. The main results are the following:

- Except for the LPSO with 10H type structure, all compounds presented faster H<sub>2</sub> generation than pure Mg and over 80% reaction yield within one hour. This result was attributed to the

presence of TM-RE noble clusters in the structure, enhancing the corrosion through galvanic coupling with Mg.

- The series of samples containing both Mg and LPSO phases were found to exhibit the highest reactivity. It was attributed to galvanic coupling between these two phases. This observation was made both in hydrolysis experiments and  $J_{\text{corr}}$  determination with electrochemical technique.
- Activation energies of 27.3 and 85.4 kJ/mol are reported for 14H+Mg ( $\text{Mg}_{91}\text{Ni}_4\text{Y}_5$  500°C 10d) and 18R-Cu ( $\text{Mg}_{83.3}\text{Cu}_{7.2}\text{Y}_{9.5}$ ) respectively. Particularly low activation energy values are obtained for [LPSO + Mg] compounds even without morphological optimization (*i.e.* without ball-milling).
- Open circuit potentials were measured and a linear variation of alloy's OCP with Mg content was observed.

While the differences induced by the LPSO type remain unclear, the cluster composition (Mg insertion/substitutions, nature of RE/TM) seems to be the key factor for  $\text{H}_2$  generation of LPSO. Further local electrochemical studies are under progress to help evidencing their role regarding the hydrogen generation behavior and understanding electrochemical interactions between LPSO and Mg phase.

## Acknowledgment

This work was financially supported by Direction Générale de l'Armement and Région Nouvelle Aquitaine through a grant to Manuel Legrée. Catherine Denage and Dominique Denux are acknowledged for their assistance with density measurements.

## References

- [1] A. Inoue, Y. Kawamura, M. Matsushita, K. Hayashi, J. Koike, Novel hexagonal structure and ultrahigh strength of magnesium solid solution in the Mg–Zn–Y system, *J. Mater. Res.* 16 (2001) 1894–1900. <https://doi.org/10.1557/JMR.2001.0260>.
- [2] D. Xu, E.H. Han, Y. Xu, Effect of long-period stacking ordered phase on microstructure, mechanical property and corrosion resistance of Mg alloys: A review, *Prog. Nat. Sci. Mater. Int.* 26 (2016) 117–128. <https://doi.org/10.1016/j.pnsc.2016.03.006>.

- [3] P. Cheng, Y. Zhao, R. Lu, H. Hou, Effect of the morphology of long-period stacking ordered phase on mechanical properties and corrosion behavior of cast Mg-Zn-Y-Ti alloy, Elsevier B.V., 2018. <https://doi.org/10.1016/j.jallcom.2018.06.056>.
- [4] Y. Zhang, W. Liu, J. Zhang, W. Zhu, Q.Q. Ma, X.M. Zong, C.X. Xu, Influence of micro-alloying with Cd on growth pattern, mechanical properties and microstructure of as-cast Mg 94 Y 2.5 Zn 2.5 Mn 1 alloy containing LPSO structure, *Mater. Sci. Eng. A.* 748 (2019) 294–300. <https://doi.org/10.1016/j.msea.2019.01.098>.
- [5] Z. Li, F. Liu, A. Yuan, B. Duan, Y. Li, X. Li, Effect of rolling deformation on microstructure and texture of spray-deposited magnesium alloy containing Mg-Nd-Zn typed LPSO, *J. Mater. Sci. Technol.* 33 (2017) 630–636. <https://doi.org/10.1016/j.jmst.2017.02.003>.
- [6] K. Kishida, K. Nagai, A. Matsumoto, A. Yasuhara, H. Inui, Crystal structures of highly-ordered long-period stacking-ordered phases with 18R, 14H and 10H-type stacking sequences in the Mg-Zn-Y system, *Acta Mater.* 99 (2015) 228–239. <https://doi.org/10.1016/j.actamat.2015.08.004>.
- [7] K. Kishida, H. Yokobayashi, H. Inui, M. Yamasaki, Y. Kawamura, The crystal structure of the LPSO phase of the 14H-type in the Mg-Al-Gd alloy system, *Intermetallics.* 31 (2012) 55–64. <https://doi.org/10.1016/j.intermet.2012.06.010>.
- [8] C.Q. Li, D.K. Xu, Z.R. Zeng, B.J. Wang, L.Y. Sheng, X.B. Chen, E.H. Han, Effect of volume fraction of LPSO phases on corrosion and mechanical properties of Mg-Zn-Y alloys, *Mater. Des.* 121 (2017) 430–441. <https://doi.org/10.1016/j.matdes.2017.02.078>.
- [9] Z. Han, K. Zhang, J. Yang, R. Wei, Y. Liu, C. Zhang, The Anodic Role of Ni-Containing LPSO Phases During the Microgalvanic Corrosion of Mg 98 Gd 1.5 Ni 0.5 Alloy, *J. Mater. Eng. Perform.* 28 (2019) 2451–2458. <https://doi.org/10.1007/s11665-019-04018-x>.
- [10] J. Wang, S. Gao, X. Liu, X. Peng, K. Wang, S. Liu, W. Jiang, S. Guo, F. Pan, Enhanced mechanical properties and degradation rate of Mg–Ni–Y alloy by introducing LPSO phase for degradable fracturing ball applications, *J. Magnes. Alloy.* 8 (2020) 127–133. <https://doi.org/10.1016/j.jma.2019.11.010>.
- [11] J. Liu, L. Yang, C. Zhang, B. Zhang, T. Zhang, Y. Li, K. Wu, F. Wang, Role of the LPSO structure in the improvement of corrosion resistance of Mg-Gd-Zn-Zr alloys, *J. Alloys Compd.* 782 (2019) 648–658. <https://doi.org/10.1016/j.jallcom.2018.12.233>.

- [12] M. Curioni, The behaviour of magnesium during free corrosion and potentiodynamic polarization investigated by real-time hydrogen measurement and optical imaging, *Electrochim. Acta.* 120 (2014) 284–292. <https://doi.org/10.1016/j.electacta.2013.12.109>.
- [13] S. Thomas, N. V. Medhekar, G.S. Frankel, N. Birbilis, Corrosion mechanism and hydrogen evolution on Mg, *Curr. Opin. Solid State Mater. Sci.* 19 (2015) 85–94. <https://doi.org/10.1016/j.cossms.2014.09.005>.
- [14] A. Atrens, G.L. Song, F. Cao, Z. Shi, P.K. Bowen, Advances in Mg corrosion and research suggestions, *J. Magnes. Alloy.* 1 (2013) 177–200. <https://doi.org/10.1016/j.jma.2013.09.003>.
- [15] M. Esmaily, J.E. Svensson, S. Fajardo, N. Birbilis, G.S. Frankel, S. Virtanen, R. Arrabal, S. Thomas, L.G. Johansson, Fundamentals and advances in magnesium alloy corrosion, *Prog. Mater. Sci.* 89 (2017) 92–193. <https://doi.org/10.1016/j.pmatsci.2017.04.011>.
- [16] E. Alasmar, I. Aubert, A. Durand, M. Nakhil, M. Zakhour, E. Gaudin, J.L. Bobet, Hydrogen generation from Mg–NdNiMg 15 composites by hydrolysis reaction, *Int. J. Hydrogen Energy.* 44 (2019) 523–530. <https://doi.org/10.1016/j.ijhydene.2018.10.233>.
- [17] S.-L. Li, J.-M. Song, J.-Y. Uan, Mg–Mg<sub>2</sub>X (X=Cu, Sn) eutectic alloy for the Mg<sub>2</sub>X nano-lamellar compounds to catalyze hydrolysis reaction for H<sub>2</sub> generation and the recycling of pure X metals from the reaction wastes, *J. Alloys Compd.* 772 (2019) 489–498. <https://doi.org/10.1016/j.jallcom.2018.09.154>.
- [18] A. Kantürk Figen, B. Coşkuner, S. Pişkin, Hydrogen generation from waste Mg based material in various saline solutions (NiCl<sub>2</sub>, CoCl<sub>2</sub>, CuCl<sub>2</sub>, FeCl<sub>3</sub>, MnCl<sub>2</sub>), *Int. J. Hydrogen Energy.* 40 (2015) 7483–7489. <https://doi.org/10.1016/j.ijhydene.2015.01.022>.
- [19] S.K. Oh, T.H. Cho, M.J. Kim, J.H. Lim, K.S. Eom, D.H. Kim, E.A. Cho, H.S. Kwon, Fabrication of Mg–Ni–Sn alloys for fast hydrogen generation in seawater, *Int. J. Hydrogen Energy.* 42 (2017) 7761–7769. <https://doi.org/10.1016/j.ijhydene.2016.11.138>.
- [20] M.H. Grosjean, M. Zidoune, L. Roué, Hydrogen production from highly corroding Mg-based materials elaborated by ball milling, *J. Alloys Compd.* 404–406 (2005) 712–715. <https://doi.org/10.1016/j.jallcom.2004.10.098>.
- [21] L.Z. Ouyang, J.M. Huang, H. Wang, Y.J. Wen, Q.A. Zhang, D.L. Sun, M. Zhu, Excellent hydrolysis performances of Mg<sub>3</sub>RE hydrides, *Int. J. Hydrogen Energy.* 38 (2013) 2973–2978.

<https://doi.org/10.1016/j.ijhydene.2012.12.092>.

- [22] M. Huang, L. Ouyang, Z. Chen, C. Peng, X. Zhu, M. Zhu, Hydrogen production via hydrolysis of Mg-oxide composites, *Int. J. Hydrogen Energy*. 42 (2017) 22305–22311.  
<https://doi.org/10.1016/j.ijhydene.2016.12.099>.
- [23] X. Hou, Y. Wang, Y. Yang, R. Hu, G. Yang, L. Feng, G. Suo, X. Ye, L. Zhang, H. Shi, L. Yang, Z.G. Chen, Enhanced hydrogen generation behaviors and hydrolysis thermodynamics of as-cast Mg–Ni–Ce magnesium-rich alloys in simulate seawater, *Int. J. Hydrogen Energy*. 44 (2019) 24086–24097. <https://doi.org/10.1016/j.ijhydene.2019.07.148>.
- [24] A. Javaid, E. Essadiqi, S. Bell, B. Davis, Literature review on magnesium recycling, *Magnes. Technol.* 2006 (2006) 7–12.
- [25] S. Al Bacha, A.S. Awad, E. El Asmar, T. Tayeh, J.L. Bobet, M. Nakhl, M. Zakhour, Hydrogen generation via hydrolysis of ball milled WE43 magnesium waste, *Int. J. Hydrogen Energy*. 44 (2019) 17515–17524. <https://doi.org/10.1016/j.ijhydene.2019.05.123>.
- [26] J.Y. Uan, C.Y. Cho, K.T. Liu, Generation of hydrogen from magnesium alloy scraps catalyzed by platinum-coated titanium net in NaCl aqueous solution, *Int. J. Hydrogen Energy*. 32 (2007) 2337–2343. <https://doi.org/10.1016/j.ijhydene.2007.03.014>.
- [27] R. Akbarzadeh, J.A. Adeniran, M. Lototsky, A. Asadi, Simultaneous brewery wastewater treatment and hydrogen generation via hydrolysis using Mg waste scraps, *J. Clean. Prod.* 276 (2020) 123198. <https://doi.org/10.1016/j.jclepro.2020.123198>.
- [28] S. Al Bacha, I. Aubert, O. Devos, M. Zakhour, M. Nakhl, J.L. Bobet, Corrosion of pure and milled Mg17Al12 in “model” seawater solution, *Int. J. Hydrogen Energy*. 45 (2020) 15805–15813.  
<https://doi.org/10.1016/j.ijhydene.2020.04.030>.
- [29] S. Al Bacha, I. Aubert, M. Zakhour, M. Nakhl, J.-L. Bobet, Hydrolysis properties, corrosion behavior and microhardness of AZ91 “model” alloys, *J. Alloys Compd.* 845 (2020) 156283.  
<https://doi.org/10.1016/j.jallcom.2020.156283>.
- [30] J.Y. Uan, M.C. Lin, C.Y. Cho, K.T. Liu, H.I. Lin, Producing hydrogen in an aqueous NaCl solution by the hydrolysis of metallic couples of low-grade magnesium scrap and noble metal net, *Int. J. Hydrogen Energy*. 34 (2009) 1677–1687. <https://doi.org/10.1016/j.ijhydene.2008.11.097>.
- [31] A.S. Awad, E. El-Asmar, T. Tayeh, F. Mauvy, M. Nakhl, M. Zakhour, J.L. Bobet, Effect of carbons

- (G and CFs), TM (Ni, Fe and Al) and oxides (Nb<sub>2</sub>O<sub>5</sub> and V<sub>2</sub>O<sub>5</sub>) on hydrogen generation from ball milled Mg-based hydrolysis reaction for fuel cell, *Energy*. 95 (2016) 175–186. <https://doi.org/10.1016/j.energy.2015.12.004>.
- [32] M.H. Grosjean, L. Roué, Hydrolysis of Mg-salt and MgH<sub>2</sub>-salt mixtures prepared by ball milling for hydrogen production, *J. Alloys Compd.* 416 (2006) 296–302. <https://doi.org/10.1016/j.jallcom.2005.09.008>.
- [33] S.A. Pighin, G. Urretavizcaya, J.L. Bobet, F.J. Castro, Nanostructured Mg for hydrogen production by hydrolysis obtained by MgH<sub>2</sub> milling and dehydriding, *J. Alloys Compd.* 827 (2020). <https://doi.org/10.1016/j.jallcom.2020.154000>.
- [34] J. Liu, C. Zou, H. Wang, L. Ouyang, M. Zeng, M. Zhu, Enhancing effect of LPSO phases on hydrogen ab- and desorption kinetics of Mg<sub>94</sub>Cu<sub>4</sub>Y<sub>2</sub> alloy, *Cailiao Yanjiu Xuebao/Chinese J. Mater. Res.* 30 (2016) 248–254. <https://doi.org/10.11901/1005.3093.2015.189>.
- [35] M. Jiang, S. Zhang, Y. Bi, H. Li, Y. Ren, G. Qin, Phase equilibria of the long-period stacking ordered phase in the Mg-Ni-Y system, *Intermetallics*. 57 (2015) 127–132. <https://doi.org/10.1016/j.intermet.2014.10.014>.
- [36] V. Charbonnier, K. Asano, H. Kim, K. Sakaki, Hydrogenation Properties of Mg<sub>83.3</sub>Cu<sub>7.2</sub>Y<sub>9.5</sub> with Long Period Stacking Ordered Structure and Formation of Polymorphic  $\gamma$ -MgH<sub>2</sub>, *Inorg. Chem.* (2020) 0–11. <https://doi.org/10.1021/acs.inorgchem.0c02080>.
- [37] D. Egusa, E. Abe, Structure of long-period stacking / order Mg-Zn-RE (RE : rare-earth and Y) phases with extended non-stoichiometry ranges, (n.d.).
- [38] X. Hou, H. Shi, L. Yang, L. Feng, G. Suo, X. Ye, L. Zhang, Y. Yang, Comparative investigation on feasible hydrolysis H<sub>2</sub> production behavior of commercial Mg-M (M = Ni, Ce, and La) binary alloys modified by high-energy ball milling—Feasible modification strategy for Mg-based hydrogen producing alloys, *Int. J. Energy Res.* (2020) 1–17. <https://doi.org/10.1002/er.5843>.
- [39] P. Liu, H. Wu, C. Wu, Y. Chen, Y. Xu, X. Wang, Y. Zhang, Microstructure characteristics and hydrolysis mechanism of Mg-Ca alloy hydrides for hydrogen generation, *Int. J. Hydrogen Energy*. 40 (2015) 3806–3812. <https://doi.org/10.1016/j.ijhydene.2015.01.105>.
- [40] Z.H. Tan, L.Z. Ouyang, J.M. Huang, J.W. Liu, H. Wang, H.Y. Shao, M. Zhu, Hydrogen generation via hydrolysis of Mg<sub>2</sub>Si, *J. Alloys Compd.* 770 (2019) 108–115.

<https://doi.org/10.1016/j.jallcom.2018.08.122>.

- [41] E. Alasmar, A.S. Awad, D. Hachem, T. Tayeh, M. Nakhl, M. Zakhour, E. Gaudin, J.L. Bobet, Hydrogen generation from Nd-Ni-Mg system by hydrolysis reaction, *J. Alloys Compd.* 740 (2018) 52–60. <https://doi.org/10.1016/j.jallcom.2017.12.305>.
- [42] F. Xiao, Y. Guo, R. Yang, J. Li, Hydrogen generation from hydrolysis of activated magnesium/low-melting-point metals alloys, *Int. J. Hydrogen Energy.* 44 (2019) 1366–1373. <https://doi.org/10.1016/j.ijhydene.2018.11.165>.
- [43] M. Yamasaki, M. Matsushita, K. Hagihara, H. Izuno, E. Abe, Y. Kawamura, Highly ordered 10H-type long-period stacking order phase in a Mg-Zn-Y ternary alloy, *Scr. Mater.* 78–79 (2014) 13–16. <https://doi.org/10.1016/j.scriptamat.2014.01.013>.
- [44] E. Al Asmar, S. Tencé, J.L. Bobet, B. Ourane, M. Nakhl, M. Zakhour, E. Gaudin, The Mg-Rich Phase NdNiMg15: Structural and Magnetic Properties, *Inorg. Chem.* 57 (2018) 14152–14158. <https://doi.org/10.1021/acs.inorgchem.8b02007>.